ISSN 1070-3632, Russian Journal of General Chemistry, 2011, Vol. 81, No. 11, pp. 2332–2344. © Pleiades Publishing, Ltd., 2011.
Original Russian Text © V.A. Minaeva, B.F. Minaev, G.V. Baryshnikov, T.N. Kopylova, R.M. Gadirov, N.S. Eremina, 2011, published in Zhurnal Obshchei Khimii, 2011, Vol. 81, No. 11, pp. 1881–1893.

Study of Structure and Spectral Characteristics of the Binuclear Zinc Complex with (*E*)-2-({2-[3-(pyridin-2-yl)-1*H*-1,2,4-triazol-5-yl]phenylimino}methyl)phenol

V. A. Minaeva[a], B. F. Minaev[a], G. V. Baryshnikov[a], T. N. Kopylova[b], R. M. Gadirov[b], and N. S. Eremina[b]

[a] *Khmelnitskii Cherkassy National University, ul. Shevchenko 81, Cherkassy, 18031 Ukraine*
e-mail: minaeva@cdu.edu.ua

[b] *Tomsk State University, Tomsk, Russia*

Received October 7, 2010

Abstract—A study of the structure and spectral properties of the compound (*E*)-2-({2-[3-(pyridin-2-yl)-1*H*-1,2,4-triazol-5-yl]phenylimino}methyl)phenol and its binuclear complex with zinc was carried out by the quantum-chemical calculations at a level of density functional theory. Within the framework of the time-dependent density functional theory were calculated electron spectra of both compounds, which gave good agreement with experiment, and was revealed the nature of the absorption bands in the visible and near UV region taking into account the solvent effect. Complete interpretation of the absorption bands in the infrared spectra of the complex and protonated ligand was given, and the frequency shift and changes in the intensities of IR bands of the ligand at the complex formation were analyzed.

DOI: 10.1134/S1070363211110193

The organometallic structures capable of the effective mutual transformation of electric and light energy, have attracted much attention of researchers in different fields of science and technology [1–4]. This is due primarily to the development of technology of organic light-emitting diodes used in microelectronics, whose operating principle is based on the ability of an organic or organometallic compound to electro-luminescence. Such requirements are satisfied by the synthesized earlier 1,2,4-triazole derivative, (*E*)-2-({2-[3-(pyridin-2-yl)-1*H*-1,2,4-triazol-5-yl]phenylimino}-methyl)phenol (H_2L) [5]. Electroluminescence of a sensor devices based on this compound and its binuclear complex with zinc (Zn_2L_2) has been studied [6], and the complex Zn_2L_2 was shown to exhibit a more stable electroluminescence and is more resistant to oxidation (burning out) than the compound H_2L.

This paper concerns the results of quantum-chemical study of the structure and spectral properties of the compound H_2L and its binuclear complex with zinc (Zn_2L_2). The data obtained explain the influence of complexation on the structure and spectral properties of these compounds. On the basis of the calculations we revealed the nature of compound H_2L and its complex absorption in the visible and infrared regions, which can be useful in designing new electroluminescent devices. A detailed study of IR spectra allowed us to determine the nature of all the bands, as well as to trace the changes in the frequencies and intensities of infrared absorption at the complexation. This provides additional criteria for establishing the relationship between the structure of the compounds, the nature of complex formation, and their electronic and photophysical properties.

Analysis of the Structure of Molecular Complex Zn_2L_2 and Protonated Ligand H_2L

Optimized structure of the complex Zn_2L_2 is shown in Fig. 1. All calculated frequencies in the vibration spectrum of the complex are real, indicating that it corresponds to the true global minimum on the potential energy hypersurface of the molecule.

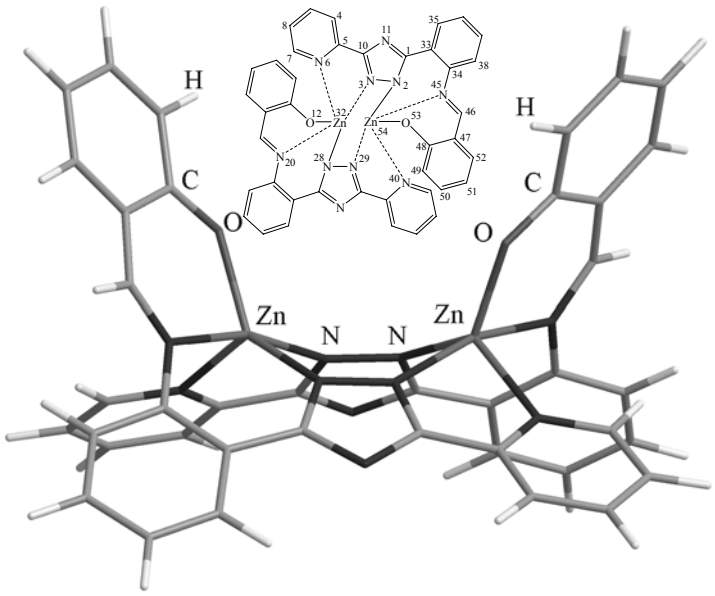

Fig. 1. Optimized molecular structure of the complex of zinc with (*E*)-2-({2-[3-(pyridin-2-yl)-1*H*-1,2,4-triazol-5-yl]phenylimino}-methyl)phenol.

The results of X-ray diffraction studies of single crystals of the complex $[Zn_2L_2]\cdot 0.5C_2H_5OH$ [5] indicate that the complex has a binuclear structure. Zinc ions are coordinated by two pentadentate ligands in the deprotonated form (L^{2-}). Each zinc atom is located inside a distorted tetragonal pyramid: it base includes four nitrogen atoms and at the top is phenolic oxygen atom. The DFT optimized structure of Zn_2L_2 complex (Fig. 1) agrees well with X-ray analysis [5].

As seen from Fig. 1, the central six-membered metallocycle Zn_2N_4 has *bath* conformation, in agreement with X-ray study [5]. The zinc atoms are located out of the plane of four nitrogen atoms at 1.459 Å in the direction of the oxygen atoms. The Zn^{32}–Zn^{54} distance equals 4.074 Å, which is close to the experimental data (4.038 Å [5]). Planar phenyl and pyridyl fragments are quasi-coplanar with the plane of the triazole fragment. Thus, the calculated dihedral angles $C^4C^5C^{10}N^{11}$ and $C^{35}C^{33}C^1N^{11}$ are –9.7° and 9.4°, respectively, and the angles $N^6C^5C^{10}N^3$ and $C^{34}C^{33}C^1N^2$ are –6.3° and 14.1°. The 2-iminomethylphenol fragment is almost planar (angle $N^{45}C^{46}C^{47}C^{52}$ equals 176.9°) and is turned by 45° to the benzene ring (angle $C^{38}C^{34}N^{45}C^{46}$ is 44.97°). The calculated bond lengths and bond angles for the Zn_2L_2 coordination sphere and those obtained experimentally for the solvate complex $[Zn_2L_2]\cdot 0.5C_2H_5OH$ are given in Table 1. Table 2 compares the calculated bond lengths and bond angles for the H_2L and Zn_2L_2 molecules (the shown parameters are those changed in bond length at the complex formation not less than 0.002 Å, in bond angle not less than 2°).

As seen from Table 1, the related geometric parameters of the coordination spheres of both zinc ions are equal, that is not fully consistent with the experimental data. This is due to the fact that the X-ray analysis was performed for the solvate complex $[Zn_2L_2]\cdot 0.5C_2H_5OH$ in which ethanol molecules are coordinated through the phenolic oxygen atom of one of the ligands, which slightly distorts the geometry of the coordination sphere of one zinc ion in comparison with other. Pentacoordinated environment of each zinc ion is composed of two ionic bonds [$Zn^{32(54)}$–$O^{12(53)}$, $Zn^{32(54)}$–$N^{28(2)}$], which compensate the positive charge of Zn^{2+} and provide electroneutrality of the complex. The three remaining bonds Zn–N are the coordination bonds of the donor–acceptor type due to the lone electron pairs of nitrogen atoms and three vacant 4*p*-AO of zinc ions. The Zn–N coordination bonds are not equal, due to the peculiarities of the geometric and electronic structure of the H_2L molecule: the length of the zinc ion bond with the pyridyl nitrogen [$Zn^{32(54)}$–$N^{6(40)}$] is 2.205 Å, with azomethine nitrogen [$Zn^{32(54)}$–$N^{20(45)}$] 2.139 Å, and with triazole nitrogen [$Zn^{32(54)}$–$N^{3(29)}$] 2.096 Å. From the obtained bond lengths can be judged their strength. The participation of the azomethine nitrogen in the formation of coordination bond led to the loss of the *p*–π-conjugation between

Table 1. Calculated and experimental bond lengths (Å) and bond angles (deg) of the coordination sphere of the zinc complex with (*E*)-2-{[2-(3-(pyridin-2-yl)-1*H*-1,2,4-triazol-5-yl)phenylimino]methyl}phenol

Bond, angle[a]	Calculation	Experiment [5]
$Zn^{32}N^{3}$	2.096	2.094
($Zn^{54}N^{29}$)	2.096	2.072
$Zn^{32}N^{6}$	2.205	2.171
($Zn^{54}N^{40}$)	2.205	2.145
$Zn^{54}N^{2}$	2.047	2.052
($Zn^{32}N^{28}$)	2.047	2.043
$Zn^{54}N^{45}$	2.139	2.113
($Zn^{32}N^{20}$)	2.139	2.101
$Zn^{54}O^{53}$	1.923	1.923
($Zn^{32}O^{12}$)	1.923	1.922
$Zn^{54}Zn^{32}$	4.074	4.038
$O^{53}Zn^{54}N^{2}$	130.61	126.62
($O^{12}Zn^{32}N^{28}$)	130.60	129.75
$O^{53}Zn^{54}N^{29}$	105.84	102.12
($O^{12}Zn^{32}N^{3}$)	105.86	100.16
$N^{2}Zn^{54}N^{29}$	88.45	87.90
($N^{28}Zn^{32}N^{3}$)	88.45	89.54
$O^{53}Zn^{54}N^{45}$	90.24	92.20
($O^{12}Zn^{32}N^{20}$)	90.25	93.70
$N^{2}Zn^{54}N^{45}$	82.92	81.83
($N^{20}Zn^{32}N^{28}$)	82.93	82.97
$N^{3}Zn^{32}N^{20}$	163.66	166.05
($N^{29}Zn^{54}N^{45}$)	163.69	165.55
$O^{53}Zn^{54}N^{40}$	100.90	108.33
($O^{12}Zn^{32}N^{6}$)	100.90	100.65
$N^{2}Zn^{54}N^{40}$	128.49	125.01
($N^{28}Zn^{32}N^{6}$)	128.50	129.46
$N^{6}Zn^{32}N^{3}$	75.71	76.10
($N^{29}Zn^{54}N^{40}$)	75.71	71.51
$N^{20}Zn^{32}N^{6}$	98.92	99.68
($N^{40}Zn^{54}N^{45}$)	98.96	100.15

[a] In parentheses are given the analogous parameters for the second ligand.

the nitrogen lone pair and benzene ring, which is reflected by the bond length $C^{21(34)}$–$N^{20(45)}$ (1.426 Å in H_2L and 1.440 Å in Zn_2L_2) .

The greatest changes in the bond lengths and bond angles at the complex formation occur in imino-methylphenol fragment and triazole ring (Table 2), as a result of deprotonation of (*E*)-2-{[2-(3- (pyridin-2-yl)-1*H*-1,2,4-triazol-5-yl)phenylimino]methyl}phenol at the complex formation and the redistribution of electron density in the ligand due to coordination with

Table 2. Calculated bond lengths (Å) and bond angles (deg) changed upon complexation, in the protonated ligand H_2L and complex Zn_2L_2

Bond, angle	H_2L	Zn_2L_2
$C^{4}C^{5}$	1.395	1.387
$C^{5}N^{6}$	1.342	1.351
$C^{7}C^{8}$	1.389	1.385
$C^{5}C^{10}$	1.453	1.442
$C^{10}N^{11}$	1.369	1.345
$C^{1}N^{11}$	1.333	1.356
$N^{2}N^{3}$	1.358	1.355
$C^{1}C^{33}$	1.447	1.451
$C^{34}N^{45}$	1.406	1.420
$N^{45}C^{46}$	1.284	1.307
$C^{46}C^{47}$	1.448	1.420
$C^{47}C^{48}$	1.399	1.431
$C^{48}O^{53}$	1.380	1.302
$C^{48}C^{49}$	1.387	1.414
$C^{49}C^{50}$	.385	1.371
$C^{50}C^{51}$	1.391	1.405
$C^{51}C^{52}$	1.381	1.369
$C^{52}C^{47}$	1.397	1.413
$C^{1}N^{2}N^{3}$	111.6	106.6
$N^{2}N^{3}C^{10}$	102.1	106.1
$N^{2}C^{1}N^{11}$	108.2	111.4
$C^{10}N^{11}C^{1}$	104.5	111.4
$C^{5}C^{10}N^{11}$	122.1	128.6
$N^{11}C^{1}C^{33}$	126.2	124.1
$N^{3}C^{10}C^{5}$	124.3	118.5
$C^{10}C^{5}N^{6}$	118.3	114.8
$C^{10}C^{5}C^{4}$	119.3	123.4
$C^{33}C^{34}N^{45}$	118.9	121.3
$C^{38}C^{34}N^{45}$	122.1	119.8
$C^{34}N^{45}C^{46}$	121.7	117.6
$N^{45}C^{46}C^{47}$	122.2	116.5
$C^{46}C^{47}C^{48}$	119.8	124.4
$C^{47}C^{48}O^{53}$	117.1	123.3
$O^{53}C^{48}C^{49}$	121.8	119.1

zinc ions. Thus, in iminomethylphenol fragment the length of $C^{13(48)}$–$C^{18(47)}$ bond increases by 0.032 Å, $C^{13(48)}$–$O^{12(53)}$ decreases by 0.078 Å, $C^{18(47)}$–$C^{19(46)}$ decreases by 0.028 Å, $C^{19(46)}$–$N^{20(45)}$ increases by 0.023 Å. In the triazole ring the $C^{1(27)}$–$N^{11(31)}$ bond length increases by 0.023 Å, and the bond $C^{10(30)}$–$N^{11(31)}$ decreases in te length by 0.024 Å. The bond length of $N^{2(28)}$–$N^{3(29)}$ decreases by only 0.003 Å. Because of these changes, in the bound triazole ring occurs a strong deformation of the aromatic 6π-electron system, and in iminophenol fragment, along with the redistribution of electron density in the aromatic ring and donating it onto the phenolic oxygen atom and the azomethine group, is formed a system of conjugated bonds $C^{18}C^{19}N^{20}$. These changes in the structure of the molecule H_2L at the complex formation are reflected in the spectral properties of the Zn_2L_2 complex.

Analysis of the IR Absorption Spectra of the Molecular Complex Zn_2L_2 and Compound H_2L

Describing the IR absorption spectra of the molecules we used the continuous numbering of all normal modes in accordance with increasing frequencies. For indication of assignment of the vibrations we used common literal designations (Table 3).

The vibration spectrum of molecules H_2L and Zn_2L_2 have respectively 117 and 234 normal modes. Most of them are listed and interpreted in Table 3. Figure 2 compares the experimental and theoretically calculated infrared spectra of the molecules in the most important spectral range of 1650–400 cm^{-1}. The vibration frequencies of identical bonds (or groups of atoms) in the first and second ligands of the complex usually are pairwise degenerate. Number of a pair mode, its frequency and intensity are given in Table 3 in parentheses.

Comparison of experimental and theoretically calculated IR spectra (Fig. 2) shows that some experimental bands are shifted to either larger, or lower frequencies. This is especially true for the compound H_2L, which, in our opinion, is due to the intermolecular interactions in the solid compound and the influence of the crystal lattice. Accounting for this situation, to estimate the effect of complexation on the nature of the absorption bands we compared the calculated IR spectra of the complex and the H_2L compound (absorption frequency and intensity).

Vibrations of COH and COZn fragments. Presence of hydroxyl groups in the molecule H_2L leads to the appearance of absorption bands associated with vibrations of O–H and C–O bond. The characteristic frequency of the O–H bond stretching vibrations in the H_2L molecule, according to our calculations, should occur at 3525 cm^{-1} (I = 60.7 km mol^{-1}). In the experimental IR spectrum of H_2L this band is shifted to lower frequencies (3213 cm^{-1}), which is typical for the polyassociates [7].

The presence of C–O bond induces appearance in the experimental IR spectrum of H_2L of strong bands

Table 3. The calculated and experimental frequencies (ν, cm^{-1}) and IR intensities (I, km mol^{-1}) of normal vibrations of the complex Zn_2L_2 and protonated ligand H_2L in the region of 1650–400 cm^{-1}

Vibration mode [a]	Zn_2L_2				H_2L			
	mode	ν_{calc}	ν_{exp}	I	mode	ν_{calc}	ν_{exp}	I
$\nu_s(C{=}C)_{Benz}$, $\nu_s(C{=}C)_{Ph}$, ν(CH=N), ν_s(C=C and C=N)$_{Py}$, $\nu_s(C{=}N)_{Trz}$, $\nu(C_{Py}–C_{Trz})$, $\nu(C_{Benz}–C_{Trz})$	204 (203)	1599	″	28.3 (14.5)	100	1597	″	14.2
$\nu_s(C{=}C)_{Benz}$, $\nu_s(C{=}C)_{Ph}$, ν(CH=N), $\delta(CH)_{Azm}$	202 (201)	1576	1576	162.6 (39.3)	99	1585	″	40.9
ν_s(C=C and C=N)$_{Py}$, $\nu_s(C{=}C)_{Ph,Benz}$, $\nu_s(C{=}N)_{Trz}$ semiring, $\nu(C_{Py}–C_{Trz})$, $\nu(C_{Benz}–C_{Trz})$ [ν(CH=N), δ(COH)]	206 (205)	1605	1591	24.5 (241.8)	98	1583	1595	63.1
ν(CH=N), $\nu_s(C{=}C)_{Ph}$, $\nu_s(C{=}C)_{Benz}$, $\delta(CH)_{Azm}$, ν(C–O) [δ(NH), ν(C–O) not occurs]	208	1613	1612	493.6	102	1611	1628	67.1
ν(CH=N), $\nu_s(C{=}C)_{Ph}$, $\nu_s(C{=}C)_{Benz}$, $\delta(CH)_{Azm}$, ν(C–O) [δ(NH), δ(COH), ν(C–O) not occurs]	207	1611	″	127.6	101	1607	″	56.9

Table 3. (Contd.)

Vibration mode [a]	Zn_2L_2				H_2L			
	mode	ν_{calc}	ν_{exp}	*I*	mode	ν_{calc}	ν_{exp}	*I*
$\nu_s(C{=}C)_{Benz}$, $\nu_s(C{=}C)_{Ph}$, $\nu(CH{=}N)$, $\delta(CH)_{Azm}$	200 (199)	1565	″	350.5 (164.2)	97	1564	1570	77.9
$\nu_s(C{=}C$ and $C{=}N)_{Py}$	198 (197)	1559	″	1.6 (49.0)	96	1559	1549	17.1
$\nu(C_{Py}–C_{Trz})$, $\nu(C_{Benz}–C_{Trz})$, $\nu_s(C{=}N)_{Trz}$ semiring, $\nu_{as}(C{=}C)_{Benz}$, $\nu_{as}(C{=}C$ and $C{=}N)_{Py}$, $\nu_{as}(C{=}C)_{Ph}$, $\nu_{as}(C–CH{=}N)$ [δ(NH)]	196 (195)	1530 (1522)	1533	212.4 (97.8)	95	1528	1523	36.0
$\nu(C_{Py}–C_{Trz})$, $\nu(C_{Benz}–C_{Trz})$, $\nu_{as}(C{=}C$ and $C{=}N)_{Py}$, $\nu_{as}(C{=}C)_{Ph}$, $\nu_s(C{=}N)_{Trz}$ semiring [δ(COH)]	194 (193)	1517 (1516)		245.1 (192.7)	93	1486	1487	21.1
$\nu_{as}(C{=}C)_{Benz}$, $\nu_{as}(C{=}C$ and $C{=}N)_{Py}$, $\nu_s(C{=}N)_{Trz}$, $\nu(C_{Py}–C_{Trz})$, $\nu(C_{Benz}–C_{Trz})$, $\nu(C_{Benz}–N)$	192 (191)	1493	1498	23.2 (74.1)	94	1497		8.6
$\nu_{as}(C{=}C)_{Ph}$, $\nu(C_{Ph}–C)$	190 (189)	1456	1458	8.8 (170.9)	91	1442	1448	57.7
$\nu_{as}(C{=}C)_{Benz}$, $\nu_{as}(C{=}C$ and $C{=}N)_{Py}$, $\nu_s(C{=}N)_{Trz}$ semiring, $\nu(C_{Benz}–N)$, $\nu(C–O)$ [δ(NH)]	188 (187)	1443	1444	128.9 (205.3)	92	1454	1458	43.9
					90	1441		78.2
$\nu(CH{=}N)$, $\nu(C–O)$	184 (183)	1430	1435	6.0 (253.5)	–	–	–	–
$\nu_{as}(C{=}C$ and $C{=}N)_{Py}$, $\nu_s(C{=}N)_{Trz}$	182 (181)	1416	1415	1.8 (44.3)	89	1428		1.5
$\delta(CH)_{Azm}$	180 (179)	1404	″	125.5 (28.4)	87	1380	1373	69.6
							1362	
$\nu(C_{Py}–C_{Trz})$, $\nu(C_{Benz}–C_{Trz})$, deformation of the Ph-, Trz-rings	178 (177)	1398	1388	203.8 (44.1)	88	1401	1419	82.7
$\delta(CH)_{Azm,Ph}$, deformation of the Ph-ring [δ(COH)]	176 (175)	1368		123.8 (53.6)	85	1343	1336	17.6
$\nu_s(C{=}N)_{Trz}$	174 (173)	1360 (1358)	1350	3.0 (37.3)	86	1349	1349	10.3
$\nu_{as}(C{=}N)_{Trz}$, $\nu(C–O)$, deformation of the Benz- and Ph-rings [δ(COH), δ(NH), нет $\nu(C–O)$]	172 (171)	1324	1331	63.0 (0.006)	84	1325		8.3
$\nu(C–O)$, $\nu_{as}(C{=}N)_{Trz}$ [δ(COH), δ(NH), нет $\nu(C–O)$]	170 (169)	1312	1321	0.9 (62.1)	83	1308	1304	21.9
$\nu_{as}(C{=}N)_{Trz}$ semiring [δ(COH)]	168 (167)	1291	1287	39.5 (22.1)	82	1295	1290	46.9
[δ(NH), $\nu_{as}(C{=}N)_{Trz}$), ν(N–N)]	–	–	–	–	81	1288	1282	19.7
[δ(NH), $\nu_{as}(C{=}N)_{Trz}$)]	–	–	–	–	79	1260		2.8
$\nu(C–O)$, $\nu(C_{Benz}–N)$, $\delta(C_{Ph}C_{Azm}N)$	162 (161)	1250	1254	23.4 (40.2)	78	1244	1234	83.4
[τ(NH), deformation of the Ph-ring]	–	–	–	–	77	1226		27.7
$\nu(C_{Benz}–N)$, $\nu(C_{Ph}–C_{Azm})$, δ(COZn) [δ(COH)]	158 (157)	1221		2.3 (50.1)	76	1220		9.3
ν(N–N)	156 (155)	1179 (1177)		28.3 (41.3)	–	–	–	–
$\nu(C_{Benz}–N)$, $\delta(CH)_{Benz,Ph}$	152 (151)	1171	1173	85.9 (75.2)	75	1179	1184	1.1
					74	1174		1.8
					73	1171		14.0
$\delta(CH)_{Ph}$	150 (149)	1165		8.9 (10.4)	–	–	–	–
$\delta(CH)_{Py}$	148 (147)	1164		7.9 (3.2)	72	1160		4.3
$\delta(CH)_{Py}$, ν(N–N) [$\nu(C^{10}–N^{11})$, δ(NH)]	146 (145)	1154 (1152)	1147	38.5 (14.6)	71	1158	1159	26.1
$\delta(CH)_{Benz}$, ν(N–N) [$\nu(C^{10}–N^{11})$]	144 (143)	1121		21.7 (31.5)	69	1121	1107	32.9
$\delta(CH)_{Ph}$ [δ(COH)]	142 (141)	1119	1128	0.03 (66.9)	70	1143	1149	88.1
$\delta(CH)_{Benz,Py}$ [δ(COH)]	140 (139)	1090		1.7 (1.4)	68	1088	1084	16.1
Breathing of Trz ring, deformation of the Py-ring, $\delta(CH)_{Benz,Py}$ [$\nu(C–O)$, δ(COH)]	138 (137)	1070		11.2 (5.5)	67	1076	1084	26.9
					66	1071		54.5

Table 3. (Contd.)

Vibration mode [a]	Zn_2L_2				H_2L			
	mode	ν_{calc}	ν_{exp}	*I*	mode	ν_{calc}	ν_{exp}	*I*
[ν(N–N), δ(NH), ν(C–O), δ(COH)]	–	–	–	–	65	1067		40.0
Breathing of Benz-ring, deformation of the Trz-ring	136 (135)	1044	1049	10.5 (8.8)	64	1036	1053	4.4
Breathing of Trz-, Py-, Benz-rings	134 (133)	1032	1036	9.4 (20.6)	62	1028	1037	8.2
Breathing of Trz-, Py-, Benz-rings	130 (129)	1018	1016	72.6 (1.6)	–	–	–	–
Breathing of Ph-ring	128 (127)	1016		21.2 (10.2)	63	1030		2.4
$\gamma(CH)_{Ph,Azm,Benz}$	124 (123)	1001	1000	4.1 (18.1)	59	1009	1003	8.8
					58	1002		8.9
Deformation of the Py-ring – plane, breathing of Trz-, Benz-rings	120 (119)	988	990	2.7 (22.4)	–	–	–	–
$\gamma(CH)_{Benz}$	116 (115)	975		3.0 (2.8)	57	978	985	6.1
Breathing of Py-, Benz-, Trz-rings	114 (113)	970 (968)		2.8 (2.4)	52	941	930	18.7
$\gamma(CH)_{Benz}$, deformation of the Ph-ring – plane, $\delta(C_{Ph}C_{Azm}N)$ and $\delta(C_{Benz}NC_{Azm})$ [γ(NH)]	108 (107)	911	920	14.8	50	897	906	3.0
[γ(NH)]	–	–	–	–	49	876	874	91.9
$\gamma(CH)_{Ph,Benz}$	104 (103)	870	860	1.3 (10.6)	47	861	860	15.0
Deformation of the Ph-, Benz-rings – plane, $\nu(C_{Benz}–N)$, $\delta(C_{Ph}C_{Azm}N)$, ν(Zn–O) [ν(C–O)]	102 (101)	838		26.3	46	834	845	19.2
$\gamma(CH)_{Py}$, deformation of the Trz-ring – plane	100 (99)	805	800	47.8 (14.6)	45	814	798	38.5
$\gamma(CH)_{Benz}$, breathing of Ph-ring, ν(Zn–O) [ν(C–O)]	98 (97)	796		74.3 (44.6)	44	785		15.3
$\gamma(CH)_{Benz}$	96 (95)	772		14.4 (0.5)	43	777		30.5
$\gamma(CH)_{Ph}$	94 (93)	771		18.6 (90.8)	42	772		85.9
					41	769		34.5
$\gamma(CH)_{Py}$	92 (91)	763	752	65.4 (59.0)	40	756	741	38.6
$\gamma(CH)_{Ph,Py,Benz}$ [deformation of the Trz-ring – out-of-plane]	90 (89)	762		11.8 (44.9)	39	739		7.2
Deformation of the Py-, Trz-, Benz-rings – out-of-plane	86 (85)	728	727	32.3 (29.3)	38	729	725	24.7
Deformation of the Py ring – plane	84 (83)	722	722	6.8 (27.1)	37	716	696	20.4
Deformation of the Py-, Trz-, Benz-, Ph-rings – plane	80 (79)	682	687	6.1 (5.6)	35	677	681	2.2
Deformation of the Py-ring – plane	76 (75)	636	640	11.1 (4.8)	33	616		2.0
Deformation of the Ph-, Benz-rings – plane, ν(Zn–O)	74 (73)	596	604	10.0 (1.0)	34	632	631	1.6
Deformation of the Ph-, Benz-rings – plane, twist of Trz-ring	68 (67)	556	561	33.6 (15.4)	31	569	575	12.7
Deformation of the Ph-ring, $C_{Ph}C_{Azm}N$ – out-of-plane, δ(ZnOC)	58 (57)	477	496	15.8 (16.7)	26	491	488	7.8
					25	490		14.7
Deformation of the Ph-ring – out-of-plane	56 (55)	456	457	2.7 (32.9)	24	459	451	11.9
Deformation of the Ph-ring – out-of-plane	52 (51)	428	425	3.0 (1.4)	23	445	436	6.9
Deformation of the Ph-ring – out-of-plane, δ(ZnOC), $\delta(C_{Ph}C_{Azm}N)$	50 (49)	426 (423)	412	3.5 (1.6)	22	413	409	3.5

[a] (ν) is stretching vibration: (s) symmetric, (as) asymmetric. Bending vibrations: (δ) in-plane deformation vibration, (τ) twist, (γ) out-of-plane deformation vibration. The indicies: (Ph) phenolic ring; (Benz) benzene ring; (Py) pyridine ring, (Trz) triazole ring, (Azm) azomethine group.

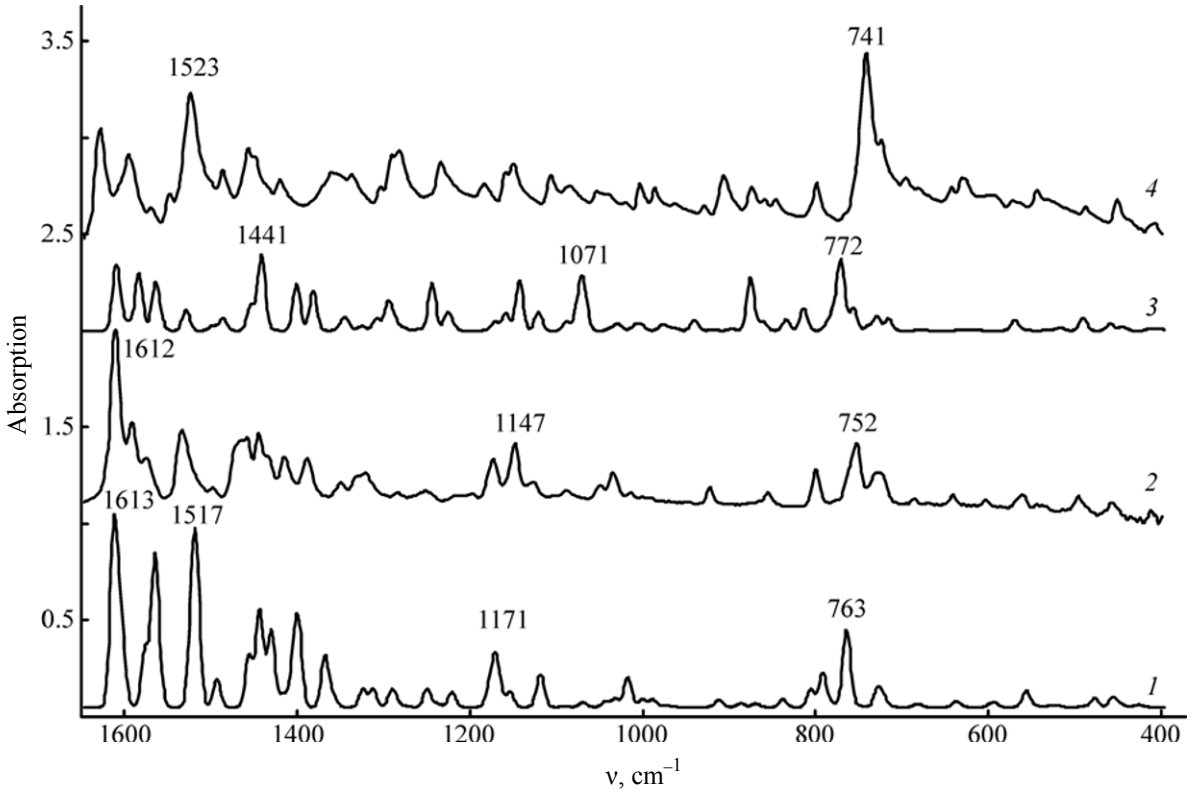

Fig. 2. (*1, 3*) Calculated and (*2, 4*) experimental IR spectra of molecules (*3, 4*) H_2L and (*1, 2*) Zn_2L_2 in 1650–400 cm^{-1}region.

at 1234 cm^{-1} (estimated: 1244 cm^{-1}, mode 78), 1084 cm^{-1} (estimated: 1071–1067 cm^{-1}, modes 66 and 65) and at 798 cm^{-1} (Fig. 2, Table 3). In the region of 1336–1290 cm^{-1} occur the plane bending vibrations of OH groups (estimated: 1343–1295 cm^{-1}, mode 85–82). In the low-frequency region there is a strong band of rocking vibrations of OH groups (ν_{calc} = 340 cm^{-1}; I = 60.7 km mol^{-1}). Formation of complex increases multiplicity of C–O bond, and in the IR spectrum of the complex in it inherent vibrations of both single bond (mode 162 (161), ν_{calc} = 1250 cm^{-1}, ν_{exp} = 1254 cm^{-1}), and at higher frequencies (exp.: 1321, 1331, 1435, 1612 cm^{-1}). The bands in which contributes vibrations of C–O bond in the frequency range 1612–1321 cm^{-1}, have greater intensity of absorption compared with the band at 1254 cm^{-1}. The band of the C–O bond stretching vibrations at 1435 cm^{-1} does not occur in the IR spectrum of H_2L.

Vibrations of the Zn–O bond occur in the frequency range 838–268 cm^{-1}. The vibrations associated with changes in the COZn angle appear at 1221 cm^{-1} [mode 58 (57)] instead of δ(COH) in the molecule H_2L, and at the frequencies below 500 cm^{-1}. Low-frequency vibrations δ(COZn) are associated with deformations of phenol rings or vibrations of the Zn–O bond.

Vibration of NH group. The characteristic absorption frequency of stretching vibrations of the N–H bond are in the region of 3500–3300 cm^{-1} [7]. According to our calculations for the molecule H_2L, a non-associated amino group of the triazole ring absorbs at 3411 cm^{-1}. Like a hydroxyl group, amino group is inclined to the formation of intermolecular hydrogen bonds, that results in the shift of the N–H stretching vibration absorption band to lower frequencies. It is well known that these shifts are smaller than for the hydroxyl group [7]. Therefore, a broad band in the experimental spectrum with a peak at 3269 cm^{-1}, in our opinion, is formed by the superposition of the absorption bands of hydroxyl and amino groups. Since the intensity of infrared N–H absorption band is much larger than that of O–H band (364.1 and 60.7 km mol^{-1}, respectively), the main peak in the first band in high-frequency region (exp. 3269 cm^{-1}) is attributed to vibrations of the amino group and weak peak (exp. 3213 cm^{-1}) to the hydroxyl group.

Plane bending vibrations of the NH group of secondary amines are usually observed in the region of 1650–1550 cm^{-1} [7]. In the calculated IR spectrum of H_2L the δ(NH) vibrations of the triazole ring are predicted in the region of 1611–1607 cm^{-1} (exp.

Table 4. The absorption maxima (λ_{max}) and their intensity (ε), the wavelengths of the vertical transitions (λ), their energies (*E*), assignment, nature and oscillator strengths (*f*) in the electron absorption spectra of the H_2L and Zn_2L_2 molecules calculated in the framework of PCM (THF) model

λ_{max}, nm	λ, nm	Assignment	*E*, eV	*f*	ε, mol^{-1} cm^{-1}	Transition nature
		H_2L				
371	371	HOMO→LUMO (84%)	3.34	0.488	5.3×10^4	S_0–S_1* π–π*
334	334	HOMO-1→LUMO (87%)	3.71	0.103	1.23×10^4	S_0–S_2* π–π*
		Zn_2L_2				
387	409	HOMO→LUMO (56%) HOMO-1→LUMO (23%)	3.03	0.079	4.16×10^4	S_0–S_1* π–π*
″	408	HOMO-1→LUMO (56%) HOMO→LUMO (20%)	3.04	0.075	″	S_0–S_2* π –π*
″	388	HOMO-1→LUMO+2 (32%) HOMO→LUMO+1 (30%)	3.20	0.132	″	S_0–S_3* π–π*
″	387	HOMO-1→LUMO+1(31%) HOMO→LUMO+2 (27%)	3.20	0.189	″	S_0–S_4* π–π*
338	340	HOMO-2→LUMO (59%) HOMO-3→LUMO+1 (20%)	3.65	0.055	1.50×10^4	S_0–S_8* π–π*
″	338	HOMO-2→LUMO+1 (39%) HOMO-3→LUMO (31%)	3.75	0.085	″	S_0–S_{10}* π–π*

1628 cm^{-1}), as well as at lower frequencies (Table 2). The absence in the Zn_2L_2 IR spectrum of the vibration modes corresponding to the NH absorption in the IR spectrum of H_2L at 1288, 1260, and 1067 cm^{-1} confirms the correctness of their assignment. Intense band at 874 cm^{-1} in the experimental IR spectrum of H_2L we assign to the out-of-plane vibrations of NH (calc. 876 cm^{-1}).

Vibrations of the azomethine group CH=N. The absorption bands of C=N systems of the type R–CH=N–R^1 are in the range of 1690–1625 cm^{-1}. Conjugation with aromatic group reduces vibration frequency of C=N bond to 1630–1615 cm^{-1} [7]. According to our calculations, the stretching vibrations of the C=N bonds in a CH=N group occur in the region 1611–1528 cm^{-1} (exp: 1628–1523 cm^{-1}). As seen from Table 4, these vibrations do not form independent bands in the infrared spectra of H_2L and Zn_2L_2, but are mixed with the vibrations of the aromatic rings and other types of vibrations, forming a band of high intensity.

Stretching vibrations of C–H bond of the azomethine group occurs at a lower frequency (estimated 2965 cm^{-1}) compared to the CH stretching vibrations in aromatic rings (estimated 3085–3000 cm^{-1}). Upon complexation, this band is shifted by 40 cm^{-1} to lower frequencies. This shift is the most clear manifestation of the coordination with the metal ion.

Plane CH bending vibrations of the azomethine group in 87 mode are not mixed with other types of vibrations, while in 85 mode are mixed with skeletal vibrations of the phenol ring to form in the experimental IR spectrum of H_2L a strong complex band with the peaks at 1362 and 1336 cm^{-1} and a shoulder at 1373 cm^{-1} (Fig. 2). The frequency of the related vibration in the complex increases by 25 cm^{-1}.

The out-of-plane CH vibrations of the azomethine groups were observed in the region of 1000 cm^{-1} (modes 59 and 58 in H_2L, 124 and 123 in Zn_2L_2). To these vibration modes contribute also the out-of-plane CH vibrations of aromatic rings. The band corresponding to these vibrations in the IR spectra of H_2L and Zn_2L_2 is weak.

Vibrations of atoms in the substituted aromatic rings. Symmetric vibrations of C=C and C=N bonds of aromatic rings in the calculated IR spectrum of H_2L induce strong bands at 1611, 1583 and 1564 cm^{-1}. To these bands also contribute C=N vibrations of

azomethine group and skeletal vibrations of C–C bond between the rings. In the experimental IR spectrum of the ligand the corresponding bands are at 1628, 1595, 1570, 1549 cm^{-1}. The calculation shows that the formation of the complex increases intensity of these bands considerably, and the band at 1595 cm^{-1}, to which contribute vibrations of C=C and C=N of the aromatic rings is shifted to higher frequencies (modes 206 and 205 in Zn_2L_2, Table 3). In the calculated infrared spectrum of the complex, this band is overlapped by the stronger band at 1612 cm^{-1}, and in the experimental IR spectrum is seen a slight shift of this band and change its shape. A weak band at 1549 cm^{-1} in the experimental IR spectrum of H_2L belonging to the symmetric C=C and C=N vibrations of pyridine (mod 96) shall not be displaced at the complex formation (modes 198 and 197), but it is overlapped by the stronger band at 1533 cm^{-1} upon complexation.

Asymmetric vibrations of aromatic C=C and C=N bonds in the calculated IR spectrum of H_2L induces absorption bands at 1528, 1486 with a shoulder at 1497 cm^{-1}, and at 1441 with a shoulder at 1454 cm^{-1}. In the experimental IR spectrum of H_2L to these vibrations correspond the strong band at 1523 cm^{-1} and 1487, 1458 and 1440 cm^{-1}. Note that the skeletal vibrations of C=N bonds in the triazole ring remain symmetric up to 1350 cm^{-1}. In the calculated IR spectrum of the complex, the asymmetric C=C and C=N vibrations are at 1530, 1517, 1493, 1456, and 1443 cm^{-1}. Based on this result, the bands in the experimental IR spectrum of Zn_2L_2 at 1533, 1498, 1458, and 1444 cm^{-1} are assigned by us to the vibrations of this type.

Asymmetric C=N vibrations in the triazole ring occur in the region 1324–1260 cm^{-1} and are not very sensitive to complex formation.

The calculated by us N–N vibrations in the triazole ring in the IR spectrum of H_2L are at 1288 cm^{-1} (mod 81) (exp: 1282 cm^{-1}). The main contribution to this mode makes the in-plane NH deformation vibration, so in the infrared spectrum of the complex the corresponding mode is missing, but there are modes of 156 (155) of medium intensity at 1179 (1177) cm^{-1} belonging to the N–N vibrations. The modes 71 and 69 in the IR spectrum of H_2L at 1158 and 1121 cm^{-1}, respectively, belong to the in-plane bending vibrations of aromatic CH bonds, and have a contribution from the C^{10}–N^{11} and N–N vibrations of the triazole ring. The IR spectrum of the complex, the related modes do not contain the contribution of $\nu(C^{10}–N^{11})$, which is associated with significant redistribution of electron density in a triazole core upon complexation, but the frequency shift and intensity change is not happening. In the region of 1084–950 cm^{-1} in the IR spectrum of the ligand and the complex appears a weak absorption bands caused by the "breath" of aromatic rings (Table 3). A significant shift of the frequencies from 941 to 968 cm^{-1} upon the complex formation shows the mode 52 [in the complex 114 (113)], belonging to the "breath" deformations in the phase of the triazole, pyridine and benzene rings, but the intensity of this mode is not sufficient (2.4 km mol^{-1}) for the observation of the corresponding bands. The phenol ring "breath" (mode 63 in the IR spectrum of H_2L), on the contrary, decreases the frequency of vibrations from 1030 cm^{-1} (H_2L) to 1016 cm^{-1} (the complex), and the intensity of absorption increases. Most intense in the IR spectrum of complex (I = 72.6 km mol^{-1}) in the given frequency range is the vibration mode 130 (calc: 1018 cm^{-1}), belonging to the "breath" oscillations (in antiphase) of triazole, pyridine and benzene rings. The corresponding mode is absent in the IR spectrum of the ligand.

In the 920–540 cm^{-1} region, in the IR spectra of the compounds observed in-plane deformation modes of aromatic rings (Table 3). Of these, it should be noted the mode 33 (pyridine ring deformation), whose frequency increases by 20 cm^{-1} at the complex formation, and the mode 34, to which along with the aromatic ring deformation contribute the Zn–O stretching vibrations, which vibration frequency decreases upon the complex formation from 631 to 604 cm^{-1}. Absorption in the region 500–350 cm^{-1} is associated with the out-of-plane deformations of aromatic rings, and below 350 cm^{-1} with the ring twisting.

The Zn–N bond vibrations. The Zn–N bond stretching vibrations occur in the low frequency region 270–160 cm^{-1} along with the aromatic rings twisting, and some modes aew very intense. Thus, the intensity of the most high of /the considered vibrations (modes 37, 36, at 268 and 249 cm^{-1}) are equal to 35 and 34 km mol^{-1}, respectively. These modes belong to the symmetric vibrations of $Zn–N_{Trz,\ semiring}$ and $Zn–N_{Py}$.

Electron Absorption Spectra of H_2L and Zn_2L_2

In the electron absorption spectrum of the H_2L compound the most intense band has a maximum at

384 nm [6]. In the spectrum of the Zn_2L_2 complex the similar band is shifted bathochromically by 23 nm and observed at 407 nm. We were able to identify these bands by (PCM) TDDFT calculations, and to establish the nature of the bands not previously described. The calculated electron absorption spectra are shown in Fig. 3.

As seen from Fig. 3, the electron spectra of compounds H_2L and Zn_2L_2 consist of two bands: a low-intensity band at short wavelength and more intense in the long-wavelength region. The long-wavelength band in the absorption spectrum of the complex is formed by two pairs of quasi-degenerate singlet-singlet excitations: 387, 388 nm and 408, 409 nm (Table 4).

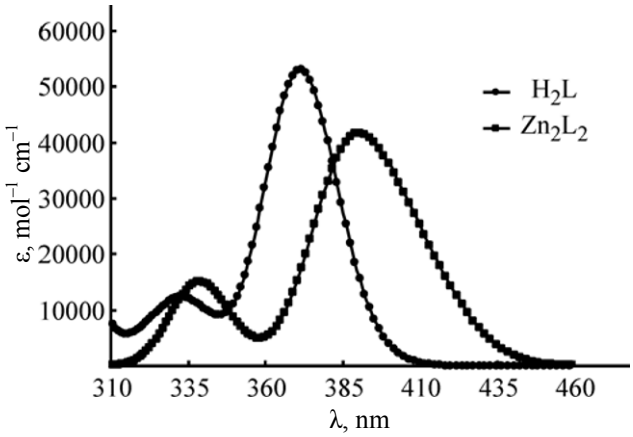

Fig. 3. Electron absorption spectra of H_2L and Zn_2L_2, molecules calculated with PCM(THF)/TDDFT/B3LYP/Lanl2DZ method.

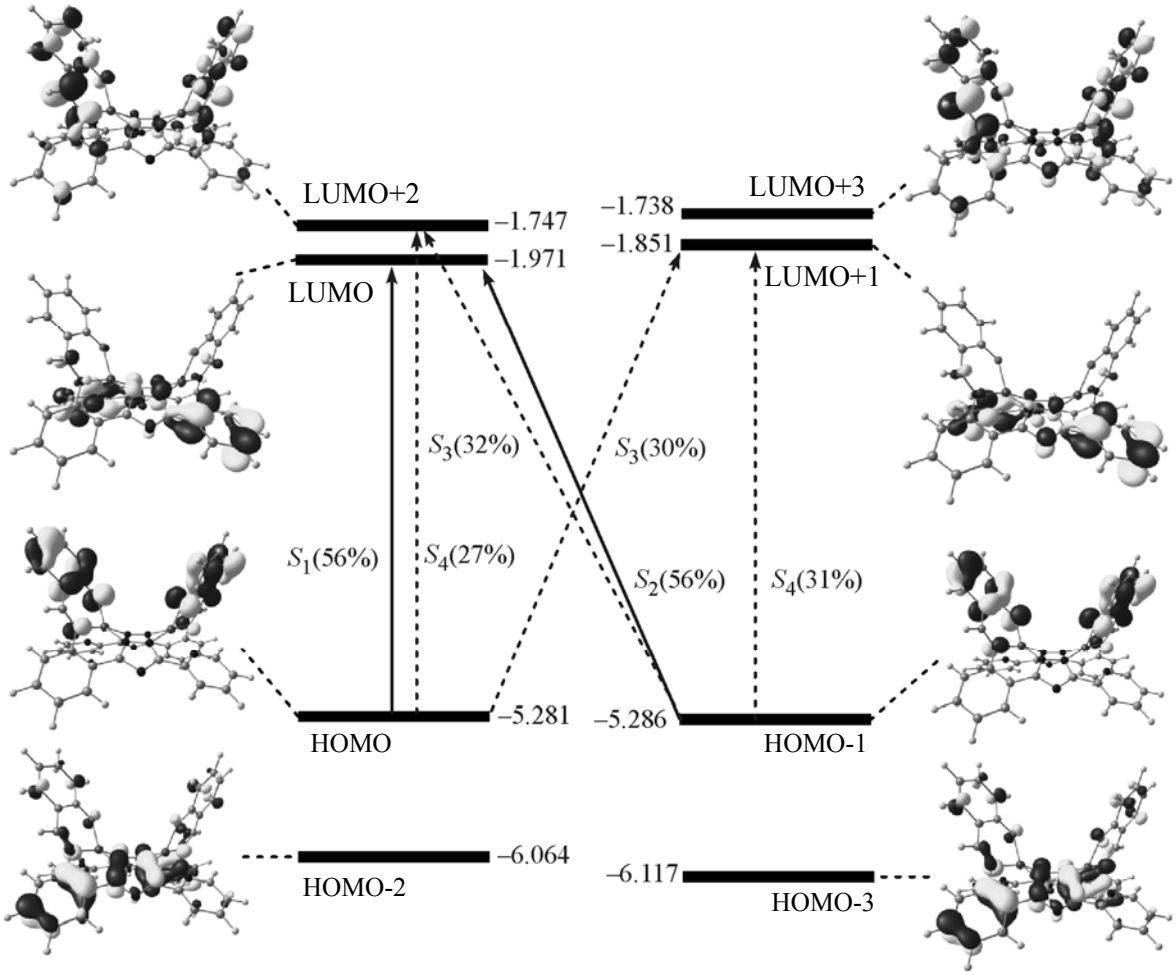

Fig. 4. Energetic diagram of the molecular orbitals of Zn_2L_2 molecule.

Electronic transitions at 387 and 388 nm are more intense and correspond to the maximum in the curve of the absorption spectrum of the complex. Excitation at 408 and 409 nm does not form a single absorption band, but increases the width and intensity of the long-wavelength band. Nature of this band can be described in terms of five-level model shown in Fig. 4. According to this model, the electronic transitions at 408 (S2) and 409 (S1) nm correspond to the one-electron $\pi \rightarrow \pi^*$ excitations HOMO-1 → LUMO (S_2) and HOMO → LUMO (S_1) with intraligand charge transfer from the phenol ring on the pyridine ring through triazole bridge. Analysis of the components of the electric dipole moment of this transition shows the possibility of charge transfer of the "ligand–ligand" type through the zinc–triazole bridge.

Electronic transitions at 387 (S_4) and 388 (S_3) nm correspond to a mixture of the configurations HOMO → LUMO+2, HOMO–1 → LUMO+1 (S_4) and HOMO–1 → LUMO+2, HOMO → LUMO+1 (S_3) in equal proportion. All configurations are of $\pi \rightarrow \pi^*$ nature, and the HOMO–1 → LUMO+1 (S_4) and HOMO → LUMO+1 (S_3) excitations occur with charge transfer, the HOMO → LUMO+2 (S_4) and HOMO–1 → LUMO+2 (S_3) excitations correspond to the intraligand redistribution of electron density (Fig. 4). These intense transitions are shifted relative to those in the ligand due to the difference of their orbital nature, and also because of the manifestation of an excimer effect of two symmetrical ligands.

Various configurations of electronic excitations from the HOMO–2 and HOMO–3 (Fig. 4) on the vacant orbitals of LUMO–LUMO+3 occur with the energy of the order of 3.65–3.80 eV and correspond to low-intensity short-wave band in the absorption spectrum of the complex (Fig. 3, Table 4) .

An intense long-wavelength band in the absorption spectrum of H_2L compound corresponds to one-electron excitation at 371 nm, which is connected with the charge transfer from the pyridine–triazole–benzene fragment on the phenol ring. Less intense shortwave band with a maximum at 334 nm is a result of singlet-singlet electronic transition defined by the charge transfer from the pyridine ring on the phenol ring.

As seen from Fig. 3, the intensity of the absorption band at 371 nm in the spectrum of H_2L is slightly higher than that of the band at 387 nm in the spectrum of the complex that does not quite match the experimental data [6]. Deviation from the experimental intensities may be due to the inadequacy of the Lanl2DZ basis in the calculation of excited states of the H_2L molecule. However, we method of calculation chosen by us gives reasonable values of the singlet-singlet excitations energies, which coincide well with the experimental data and allows reliable determining the nature of the absorption bands in the absorption spectra of the molecules.

Thus, calculation of the equilibrium geometry of the binuclear zinc complex with (*E*)-2-{[2-(3-(pyridin-2-yl)-1*H*-1,2,4-triazol-5-yl)phenylimino]methyl}phenol showed a good agreement with the data of X-ray analysis. Major changes in the structure of the ligand at the complex formation occur in iminophenol and the triazole rings, which is associated primarily with the participation of the azomethine and two triazole nitrogen atoms at the formation of coordination bonds, as well as deprotonation of phenol and triazole rings.

Detailed assignment of absorption bands in the IR spectra of compounds based on a comparison of calculated and measured IR spectra confirm the proposed structure of the complex. It is shown that the absorption bands of the IR spectrum of the complex, usually correspond to the shifted bands of the compound H_2L. Instead of the NH and OH vibrations observed in the spectrum of free ligand, in the IR spectrum of the complex appear additional bands of C–O, C=N and N=N stretching vibrations of the triazole ring and the bands of bending vibrations of aromatic rings. In the low frequency region, along with the in-plane deformations, ring twisting and displacement as well as their out-of-plane deformations, occur vibations of the coordination bonds Zn–O and Zn–N, and bending vibrations with a change in the angles involving the zinc atom.

The electron absorption spectra of the compound (*E*)-2-{[2-(3-(pyridin-2-yl)-1*H*-1,2,4-triazol-5-yl)phenylimino]methyl}phenol and its binuclear complex with zinc showed good agreement with experiment and allowed to explain the nature of the bands. We propose a five-level orbital model, which explains the nature of the absorption bands of the complex at 370–460 nm. It is assumed that the high intensity of the the first bands in the absorption spectra of the Zn_2L_2complex and H_2L compound is due to the charge-transfer excitation.

EXPERIMENTAL

The geometry optimization of the of the molecules was carried out initially by semiempirical self-

consistent field method [8] in the PM3 approximation [9], and then the resulting structural parameters were optimized based on density functional theory (DFT) using the hybrid functional B3-LYP [10, 11] in the Lanl2DZ basis [12]. For the equilibrium geometry we calculated by the same method the frequency and intensity of IR absorption bands of the molecules H_2L and Zn_2L_2, the results were compared with those in the IR spectra measured by us. Hybrid functional B3-LYP reliably predicts the vibration frequencies of organic and coordination compounds when the calculated frequencies are corrected for anharmonicity [13, 14]. This correction in our calculations was 0.9488 for the high-frequency infrared spectrum, and 0.9717 for the region 1600–400 cm^{-1}. Experimental infrared spectra of the synthesized compounds were taken from KBr matrices on a Nikolet spectrometer 380 (Thermo) in the range 4000–400 cm^{-1}. Electronic spectra were calculated in the framework of the time-dependent density functional theory (TD DFT) [15]. To simulate the effect of solvent on the electron spectra, we carried out calculations of vertical electronic excitation using the polarizable continuum model (PCM) [16]. As a model solvent was considered tetrahydrofuran (THF), which has been used in the experiment. The electron absorption spectra of solutions of the compound H_2L and the complex Zn_2L_2 in THF (c = 5.10 mol dm^{-3}) were taken on a EVOLUTION 600 (Thermo) spectrophotometer. All the experimental methods used in the study of the complex monitored directly the electron shell of the molecule. In particular, the intensity of IR bands is a sensitive criterion of changes in the polarity of bonds at the vibration deformations of the nuclear core.

The calculations were performed with the software package GAUSSIAN 03 [17] on a PDC supercomputer at the High Royal Technical School (Stockholm, Sweden). The curves profiles of the calculated IR absorption spectra of H_2L and Zn_2L_2 molecules were modeled using SWizard 4.6. program [18, 19] using the Lorentz line shape (10 cm^{-1} half-width). To construct the curves of the electron absorption spectra was applied the Gauss line shape (half-width 2000 cm^{-1}, which is typical for the UV spectra of solutions). The presence of coordination bonds Zn–N was revealed basing on the analysis of electron density distribution in the complex by the Bader method [20]. The formation of coordination bond between the two valence uncoupled atoms we fixed by the presence of a critical point (3, –1) [20]. The topology of the electron density was analyzed using the software package AIMAll [21].

ACKNOWLEDGMENTS

This work was supported in part by: the grant of Russian Foundation for Basic Research ofi-m no. 09-02-12-083 and the Federal Program “Scientific and Scientific-Pedagogical Personnel of Innovative Russia” for the years 2009–2013, in the framework of the event no. 1.2.1, State contract no. P1128.

REFERENCES

1. Hung, L.S. and Chen, C.H., *Materials Science and Engineering: R: Reports*, 2002, vol. 39, nos. 5–6, p. 143.
2. Evans, R.C., Douglas, P., and Winscom, C.J., *Coord. Chem. Rev*., 2006, vol. 250, nos. 15–16, p. 2093.
3. Chou, P.-T. and Chi, Y., *Eur. J. Inorg. Chem*., 2006, vol. 2006, no. 17, p. 3319.
4. Ding, J., Gao, J., Cheng, Y., Xie, Z., Wang, L., Ma, D., Jing, X., and Wang, F., *Adv. Funct. Mat*., 2006, vol. 16, no. 4, p. 575.
5. Gusev, A.N., Eremenko, I.L., Kiskin, M.A., and Shul’gin, V.F., *Uchenye zapiski Tavricheskogo Natsional’nogo Univ. im. V.I. Vernadskogo, seriya “Biologiya i Khimiya”* (Proceeding of Vernadskii Tavria Nat. Univ., Biology and Chemistry Series), 2009, vol. 22, no. 1, p. 154.
6. Eremina, N.S., Degtyarenko, K.M., Gadirov, R.M., Kopylova, T.N., Maier, G.V., Samsonova, L.G., Shul’gin, V.F., Gusev, A.N., Meshkova, S.B., and Minaev, B.F., *Vest. Cherkasskogo Univ.,* 2010, vol. 175, p. 100.
7. Bellamy, L.J., *The Infrared Spectra of Complex Molecules*, Moscow: Inostrannaya Literatura, 1957.
8. Dewar, M.J.S. and Theil, W., *J. Am. Chem. Soc*., 1977, vol. 99, no. 15, p. 4899.
9. Stewart, J.J.P., *J. Comp. Chem*., 1989, vol. 10, no. 2, p. 209.
10. Becke, A.D., *J. Chem. Phys*., 1993, vol. 98, no. 7, p. 5648.
11. Lee, C., Yang, W., and Parr, R.G., *Phys. Rev., B*., 1988, vol. 37, no. 2, p. 785.
12. Hay, P.J., Wadt, W.R., *J. Chem. Phys*., 1985, vol. 82, no. 1, p. 270.
13. Scott, A.P. and Radom, L., *J. Phys. Chem*., 1996, vol. 100, no. 41, p. 16502.
14. Minaev, B.F., Minaeva, V.A., Baryshnikov, G.V., Girtu, M.A., and Agren, H. , *Russ. J. Appl. Chem*., 2009, vol. 82, no. 7, p. 1211.
15. Burke, K., Werschnik, J., and Gross, E.K.U., *J. Chem. Phys*., 2005, vol. 123, no. 6, p. 062206.

16. Miertus, S., Scrocco, E., and Tomasi, J., *Chem. Phys*., 1981, vol. 55, no. 1, p. 117.

17. Frisch, M.J., Trucks, G.W., Schlegel, H.B., Scuseria, G.E., Robb, M.A., Cheeseman, J.R., Montgomeri, J.A., Jr., Vreven, T., Kudin, K.N., Burant, J.C., Millam, J.M., Iyengar, S.S, Tomasi, J., Barone, V., Mennucci, B., Cossi, M., Scalmani G, Rega, N., Petersson, G.A., Nakatsuji, H., Hada, M., Ehara, M., Toyota, K., Fukuda, R., Hasegawa, J., Ishida, M., Nakajima, T., Honda, Y., Kitao, O., Nakai, H., Klene, M., Li, X., Knox, J.E., Hratchian, H.P., Cross, J.B., Adamo, C., Jaramillo, J., Gomperts, R., Stratmann, R.E., Yazyev, O., Austin, A.J., Cammi, R., Pomelli, C., Ochterski, J.W., Ayala, P.Y., Morokuma, K., Voth, G.A., Salvador, P., Dannenberg, J.J., Zakrzewski, V.G., Dapprich, S., Daniels, A.D., Strain, M.C., Farkas, O., Malick, D.K., Rabuck, A.D., Raghavachari, K., Foresman, J.B., Ortiz, J.V., Cui, Q., Baboul, A.G., Clifford, S., Cioslowski, J., Stefanov, B.B., Liu, G., Liashenko, A., Piskorz, P., Komaromi, I., Martin, R.L., Fox, D.J., Keith, T., Al-Laham, M.A., Peng, C.Y., Nanayakkara, A., Challacombe, M., Gill, P.M.W., Johnson, B., Chen, W., Wong, M.W., Gonzalez, C., and Pople, J.A., *Gaussian 03,* Revision, C.02, Gaussian, Inc., Wallingford, CT, 2004.

18. Gorelsky, S.I., *SWizard program, http://www.sg-chem.net/,* University of Ottawa, Ottawa, Canada, 2010.

19. Gorelsky, S.I. and Lever, A.B.P., *J. Organomet. Chem*., 2001, vol. 635, nos. 1–2, p. 187.

20. Bader, R.W.F., *Atoms in Molecules. A quantum Theory*, Oxford: Clarendon Press, 1990.

21. Keitg, T.A., *AIMAII version 10.07.25, www.aim.tkgristmill.com, 2010.*